3D inversion in sub-surface electrical surveying

Michel Dabas, Alain Tabbagh, Jeanne Tabbagh

Geophys. J. Int. (1994) **119,** 975–990

3-D inversion in subsurface electrical surveying—I. Theory

M. Dabas,[1] A. Tabbagh[1,2] and J. Tabbagh[1]

[1]*Centre de Recherches Geophysiques, CNRS, 58150 Garchy, France*

[2]*Université P. et M. Curie, Laboratoire de Géophysique Appliquée, 4 place Jussieu, 75252 Paris Cedex 05, France*

Accepted 1994 June 14. Received 1994 June 6; in original form 1993 October 11

SUMMARY

The problem of 3-D inverse modelling in Direct Current (DC) surveys is addressed in this paper. First, forward modelling of the response of 3-D bodies in DC surveys is carried out by the moment method. It consists of dividing a volume into N small cells, equivalent to $3N$ dipoles. The numerical code is checked against published results obtained through algorithms that use either equivalent surface charge densities or a finite-difference approach. Good agreement is found between these methods and a maximum discrepancy of 3 per cent is computed on a widely published test model.

Secondly, inverse modelling is carried out by a classical least-squares (LS) scheme that includes the Levenberg–Marquardt constraints formalism. We have tested two approximations: Born, and localized non-linear (LN). The difference between resistivities calculated with and without these approximations is found to be too large for inverse modelling, especially in the case of conductive bodies. We use this inversion scheme for different theoretical 3-D models that consist of two layers (34 cells) under an overburden. It is found, in the case of a vertical contrast, that, when a resistive feature overlays a conductive one, resistivities are resolved very accurately, with a low number of iterations and with a better accuracy than in the case where the conductive feature overlays the resistive one. Despite a slower convergence rate, in the case of both vertical and lateral constrasts, the shape of the body is well resolved, even if a slight discrepancy in the absolute values is noticed, especially for conductive cells. Finally, the stability of the inversion is tested with noisy data.

Key words: 3-D electrical methods, 3-D inversion, least squares, moment method, surface integrals.

INTRODUCTION

The importance of subsurface surveying, which tries to image the first 10 m below the ground surface, is growing as a result of an increasing demand both in well-known fields such as civil engineering, pedology and archaeological surveying (Hesse, Jolivet & Tabbagh 1986) and in environmental geophysics. In these areas, electrical methods play an important part, since electrical resistivity in the ground (ρ) is a parameter that is easily measureable and mostly dependent upon parameters such as moisture content or texture. The variety of electrical and electromagnetic techniques that can be used for the measurement of ρ is broad: most of them can yield measurements while the instrument is moving, and at a low cost. Among these, DC electrical surveying, where a current is injected by means of electrodes in the ground and a voltage is measured with the other two electrodes, plays an important role, despite the problem of driving current into the soil when high contact resistances are encountered. This method is insensitive to the most significant problems such as natural currents or the presence of metallic objects in the vicinity of the measurement device.

The development of new technologies for rapid sampling of several channels (scanning) or multiplexing (Noel & Xu 1991; Griffiths & Turnbull 1985; Griffiths & Barker 1993; Li & Oldenburg 1992) enables quasi-simultaneous sounding (vertical variation of ρ) and profiling (lateral variations of ρ) over a short period of time. This results in a '3-D measurement' which can be used as such without loosing any part of the monitored information (Alfano 1993).

The aim of this paper is to present a 3-D inversion process

for electrical data coming from a network of electrodes. The data are resistivities acquired with different shapes and sizes of quadripoles derived from the network. Subsurface problems are generally 3-D, since the current sources are points and it is not, unfortunately, possible to lower the number of dimensions of this problem. The theoretical basis of the 3-D inverse problem is well known, but very few examples using 3-D inversion can be found in the literature. Most of them rely on approximate methods (Park & Van 1991; Shima 1992; Petrick, Sill & Ward 1981; Li & Oldenburg 1992).

Only 2-D inversion procedures have been published (Weidelt 1975; Tripp, Mohmann & Swift 1984; Smith & Vozoff 1984; Pelton, Rijo & Swift 1978; Sasaki 1989; Shima 1990; Barker 1992).

We show, in order, the forward problem, the approximations that can be used, the general 3-D inversion scheme that we have developed, and an example of synthetic data inversion with and without noise. Part II of this paper will deal with the problem of choosing the best electrode configurations and the inversion of field-derived data.

3-D FORWARD MODELLING

The most widely used method in 3-D modelling was developed by Alfano (1959): the electrical field, originating from a volume that is delimited by a closed boundary surface S and whose electrical resistivity is different from its surroundings, is approximated by a distribution of fictitious electrical charges at its boundary S. Application of the two boundary conditions, the continuity of normal components of the current density ($\mathbf{j}$) and the discontinuity of the normal component of electrical fields, yields an integral equation whose solution is the distribution of the charges. This equation is solved by delimiting the surface in N small plane surface elements, where the charge density is constant. The integral equation is then discretized in a linear system of n equations with N unknowns (if continuous functions are used, the solution becomes a Fredholm integral equation; see Okabe 1981). It is interesting to note that the 3-D problem reduces to the computation of a 2-D function. A full parametrization has been developed by Dieter, Paterson & Grant (1969) and has since been widely used for electrical or IP modelling (Barnett 1972; Spahos 1979).

This method, which belongs to the general class of boundary-value problems, can be specifically used for problems where a small number of isolated bodies are encountered in a uniform or tabular medium. For more complex bodies, where, for example, resistivity could change continuously, some theoretical problems have to be faced (Keller & Frischknecht 1966; Lee 1975), and more unknowns have to be solved for.

We have discarded this method for a general inversion scheme, both because this method cannot deal with bodies in which resistivities are not piecewise constant, and because surface charges are used instead of direct resistivities (even if the discontinuity of normal electric fields yields a direct relationship between surface charge and the contrast of resistivity).

We have not used either the finite-difference (Mufti 1978; Dey & Morrison 1979; Scriba 1981) or finite-elements methods (Pridmore *et al.* 1981) because in three dimensions they lead to systems that are much too time-consuming, even if complicated arbitrary distributions of restistivity could be modelled by these methods.

We prefer to use another approach, in which the anomalous bodies are replaced by an equivalent distribution of current sources (Das & Parasnis 1987). The theoretical basis is the same as in the case of the moment method used in electromagnetism (Raiche 1974; Hohmann 1975; Tabbagh 1985). Consequently, it can be used for simultaneous inversion of DC electric and electromagnetic data.

The total field is split into two parts; the first part is independent of the anomalous body, $\mathbf{E}_p$, and the second part results from the presence of the body, $\mathbf{E}_a$.

$\mathbf{E} = \mathbf{E}_p + \mathbf{E}_a$, and $\mathbf{H} = \mathbf{H}_p + \mathbf{H}_a$ for the magnetic field.

Let σ_s be the electrical conductivity of the body ($\rho_s = 1/\sigma_s$) and σ the conductivity of the surrounding medium (resistivity ρ). We have

$$\nabla \times \mathbf{H} = \sigma_s \mathbf{E} \quad (1) \qquad \text{and } \nabla \times \mathbf{H}_p = \sigma \mathbf{E}_p \quad (2)$$

$$\nabla \times \mathbf{E} = 0 \quad (3) \qquad \text{and } \nabla \times \mathbf{E}_p = 0 \quad (4)$$

so

$$\nabla \times \mathbf{H}_a = \sigma \mathbf{E}_a + (\sigma_s - \sigma)\mathbf{E} \quad (5)$$

and

$$\nabla \times \mathbf{E}_a = \mathbf{0}. \quad (6)$$

Consequently, the anomalous field $(\mathbf{E}_a, \mathbf{H}_a)$ can be considered as originating from a fictitious source $\mathbf{j}_s = (\sigma_s - \sigma)\mathbf{E}$. This field can be computed by the use of a potential $\mathbf{A}$ such as

$$\mathbf{H}_a = \nabla \times \mathbf{A}/\mu.$$

Using (5), one obtains

$$\mathbf{E}_a = \frac{1}{\sigma\mu} \nabla \times \nabla \times \mathbf{A} - \frac{\mathbf{j}_s}{\sigma}.$$

From eq. (6), $\mathbf{E}_a$ derives from a potential V: $\mathbf{E}_a = -\nabla V$. It becomes

$$\nabla V = \frac{-1}{\sigma\mu} \nabla \times \nabla \times \mathbf{A} + \frac{\mathbf{j}_s}{\sigma}.$$

Using the Lorentz gauge, $V = -\nabla \cdot \mathbf{A}/\sigma\mu$, we find

$$\nabla^2 \mathbf{A} = -\mu \mathbf{j}_s. \quad (7)$$

If we call $\mathscr{A}(\mathbf{r}, \mathbf{r}')$ the dyadic Green vector potential created in a layered earth at $\mathbf{r}$ by a current source of strength unity at $\mathbf{r}'$, we obtain, for the field inside a body of volume $\mathscr{V}$,

$$\mathbf{E}(\mathbf{r}) - \mathbf{E}_p(\mathbf{r}) = \int_{\mathscr{V}} \frac{\mathbf{j}_s(\mathbf{r}')}{\sigma\mu} \nabla \times \nabla \times \mathscr{A}(\mathbf{r}, \mathbf{r}')\, d\mathbf{r}' - \frac{\sigma_s - \sigma}{\sigma} \mathbf{E}(\mathbf{r}), \quad (8)$$

and outside the body we obtain

$$\mathbf{E}(\mathbf{r}) - \mathbf{E}_p(\mathbf{r}) = \int_{\mathscr{V}} \frac{\mathbf{j}_s(\mathbf{r}')}{\sigma\mu} \nabla \times \nabla \times \mathscr{A}(\mathbf{r}, \mathbf{r}')\, d\mathbf{r}'. \quad (9)$$

Integration of eq (8) by dividing the volume $\mathscr{V}$ into small cells enables us to compute the total field $\mathbf{E}$ inside each cell by solving a linear system of equations $\mathbf{TE} = \mathbf{E}_p$, where each element of the matrix $\mathbf{T}$ represents the effect of each cell on

each other cell. The computation of the effect of one cell upon itself is performed by analytical integration, which bypasses the problem of the singularity when $\mathbf{r} = \mathbf{r}'$.

For N cells we obtain $3N$ unknowns. If all the cells have the same size and σ_s is uniform inside the body, the matrix $\mathbf{T}$ is symmetrical.

NUMERICAL CHECKS

To validate this approach, we have checked the above-mentioned method, hereafter called the moment method, both with some rare 3-D numerical results already published using different approaches (surface integrals, volume integrals, finite differences) and with results produced by an older program (QUA1T) written in our laboratory using a surface-integral approach (Spahos 1979). Even if the main scope of this paper is the inversion stage, we feel that it is necessary to publish all the numerical computations of the direct problem of an already well-documented case in order to show the small discrepancies between the models.

Surface-integral approach

As mentioned above, the principle of this method is to replace the anomalous region by a distribution of electrical charges on its surface. This distribution must satisfy the two boundary conditions. By knowing the value of the normal electrical field at the injection electrode and taking the normal component to be equal to zero on the ground surface and at infinity, it can be demonstrated that the field solution of the derived equation is the unique solution of the Dirichlet problem in the case of static fields (property of harmonic fields). This method is very rapid because we have only N unknowns instead of the $3N$ unknowns of the moment method. The solution depends on the number of facets used, because the distribution of charges must be sampled on a mesh with variable size, as a consequence of the discretization process. Exact results are obtained with a dense mesh, and a compromise has to be found between the size of the mesh and the time and memory size needed for the computation.

We first made a comparison using a model that has already been used as a reference and which permits a good test of the coherence of the different approaches through: (1) a physical modelling using tank simulation performed by Endo, Takeuchi & Matsuzaka (1973). (2) Numerical resolutions computed with the same model by Okabe (1982) and Poimeur & Vasseur (1988), both of them using a surface-integral approach [a program called MODELIS, now ISTREL(BRGM)]. These results were checked against those produced by our own program QUA1T, based on the same method, and EL3DQUB, the program developed for the inversion and which uses the moment method.

The structure is a cube of resistivity 20 Ωm and length $2L$ embedded in a uniform medium of resistivity 125 Ωm. The centre of the cube is at a depth of $2L$ (see Fig. 1). A pseudo-section using dipole–dipole arrays is performed (Edwards 1977). A distance of L is kept fixed between the poles A and B, and between the poles M and N. The distance nL between B and M is increased from L (equivalent to a Wenner β configuration) to $6L$. The

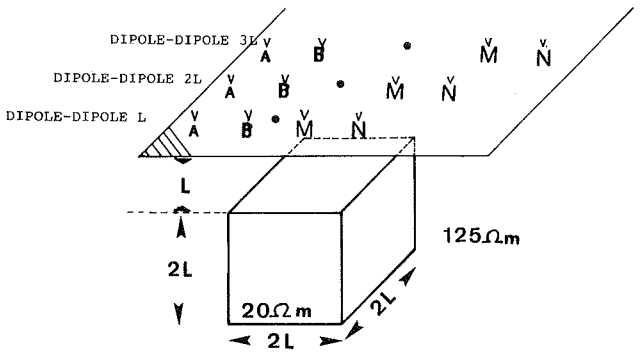

Figure 1. Model used for the numerical checks presented in Figs 2, 3 and 4. (A and B are current electrodes, M and N are potential electrodes.)

resulting apparent resistivity is plotted arbitrarily on the horizontal axis at the centre of B–M and on the vertical axis at a depth corresponding to nL.

In the upper part of Fig. 2 we plot the measurements from Endo *et al.* (1973), who uses a block of ore embedded in a sponge in a water tank. The accuracy of the resistivity measurements are thought to be near to 10 per cent.

In the middle part of Fig. 2 we plot the results of the best model from Okabe (1982, p. 669) using 216 boundary elements (each face is divided into squares of $L/3 \times L/3$) and his 'modified reciprocal averaging technique', which permits on the one hand a reciprocity that is otherwise not guaranteed in the integral equation approximations and, on the other hand, takes into account a correction term when the injection of the current is above the boundary interface. The definition of an error is not possible since he does not know if this method converges towards the exact solution (Okabe 1982, p. 669) but convergence is observed when increasing the number of boundary elements from 24 to 216: for example, he has found a maximum discrepancy of 2 per cent (2 Ωm) between the models taking into account 96 and 216 elements and a 1.2 per cent maximum reciprocal error is quoted by Okabe in the 216 elements model.

In the lower part of Fig. 2, the solution calculated by the MODELIS program, which makes no assumption about reciprocity is shown. Except for a single point, the agreement with Okabe's result is very good and the maximum discrepancy is 3 Ωm for the points above the structure.

Figure 3 shows the result of our surface-integral program QUAT1 with 216 elements (Fig. 3a) and 1000 elements (Fig. 3b). The maximum error occurs systematically when the position of the injection electrodes coincides with the projection onto the ground surface of one of the vertical interfaces of the body (highlighted as four oblique lines on the pseudo-section representation). As noticed by some authors (Okabe 1981; Das & Parasnis 1987), this is the result of the discretization of the surface and happens when the assumption of a uniform charge distribution on the small surfaces is violated. This error should be lessened by taking an equivalent configuration of the electrodes (principle of reciprocity) in which the injection electrodes do not lie above vertical interfaces: permuting ABMN to MNAB (see Fig. 1), for example, is equivalent, the structure being symmetric, to substituting the two lines a, b by c, d.

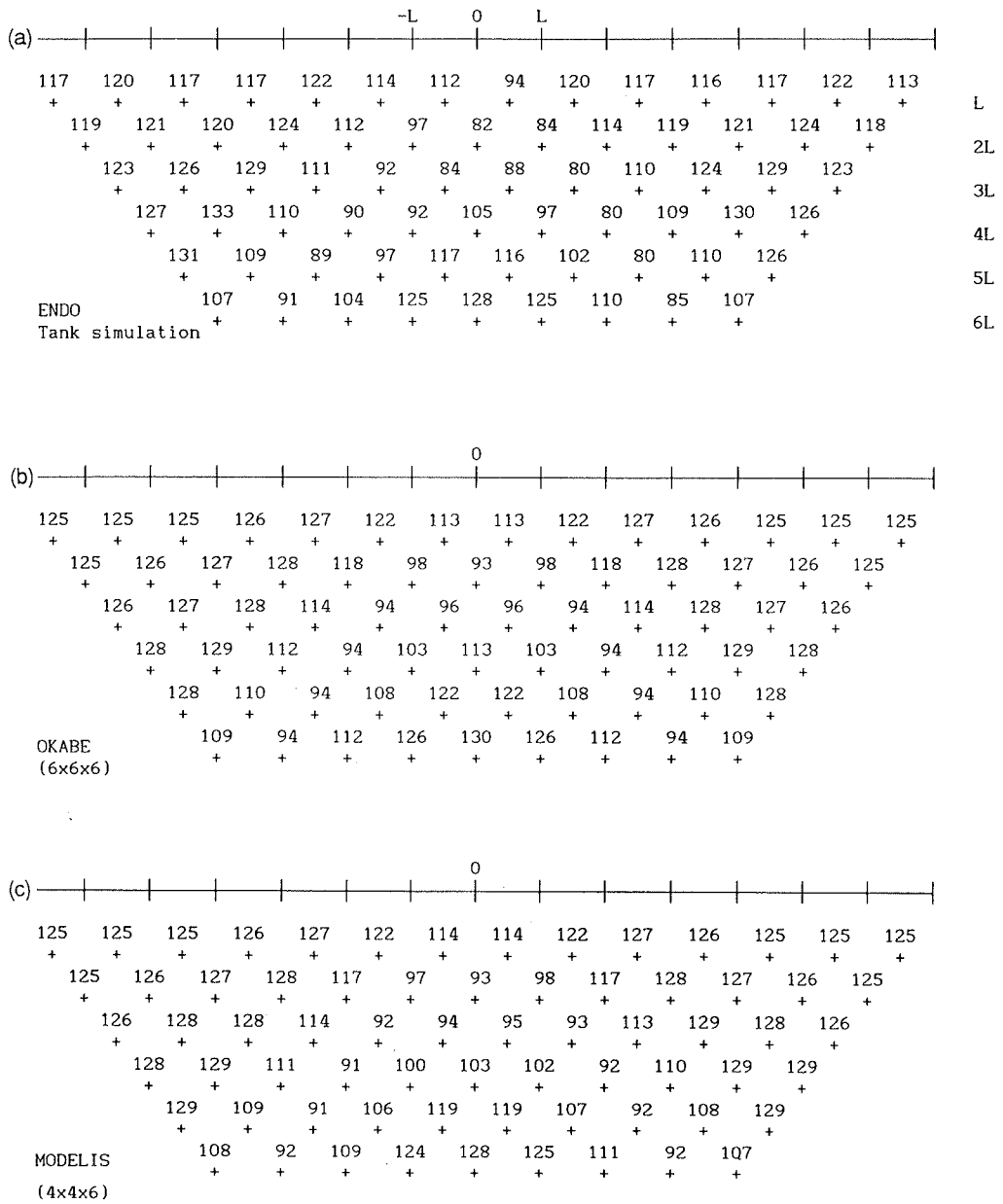

Figure 2. Electrical pseudo-sections resulting from (a) a tank simulation (Endo *et al.* 1973), (b) numerical simulation by Okabe (1982) using 216 boundary elements ($6 \times 6 \times 6$ facets) and (c) numerical simulation with the MODELIS program (Okabe 1982). To be compared with Fig. 3.

However, for reasons that are not very clear, this does not totally correct for that artefact. Increasing the number of cells provides a better solution: in the middle part of Fig. 3, the use of 600 cells leads to a better symmetry of the response. The maximum difference between these two models is low (1.0 Ωm). However, if we omit these points, the maximum discrepancy with the model of Okabe if 3 Ωm.

Volume-integral and finite-difference approaches

A comparison of the results of our program EL3DQUB (volume-integral method, Fig. 4) with those of Okabe shows that the maximum discrepancy is small: 1.5 Ωm (again, points above the vertical interfaces are excluded). The convergence of the solution can be illustrated by comparing the results using cubic cells of dimensions $0.5L$ (Fig. 4a left) and $0.33L$ (Fig. 4b right).

Finally, we have checked the results of our program EL3DQUB against numerical results coming from a similar program by Das & Parasnis (1987) using the moment method, and against a program using finite-differences (Dey & Morisson, 1979). The geometry of the model is given at the top of Fig. 5.

The definition of the size of the cells is a compromise between stability and time or storage computing requirements. The different apparent resistivities computed with the number of cells increasing from 4 to 500, and for a quadripole corresponding to $6L$, are presented in the middle part of Fig. 5.

The stability of EL3DQUB is illustrated through the very

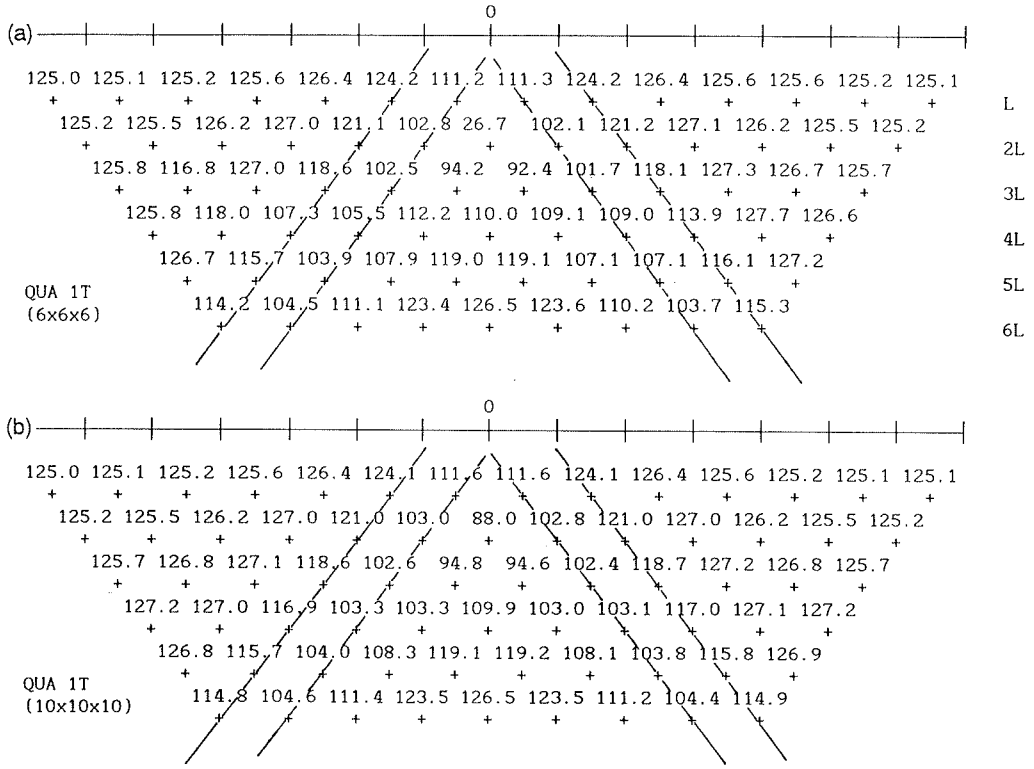

Figure 3. Electrical pseudo-sections resulting from our numerical simulations using a surface-integral approach (QUA1T) with (a) 216 boundary elements, and (b) 1000 boundary elements. Diagonal lines represent positions where the position of the electrodes coincide with the projection of the vertical faces of the body on the surface.

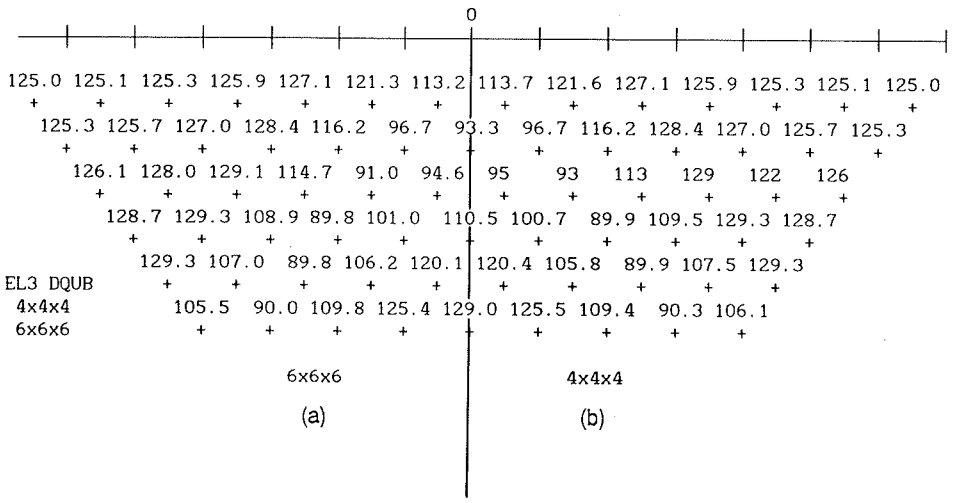

Figure 4. Comparison of electrical pseudo-sections resulting from our numerical simulations using a volume-integral approach (EL3DQUB) with (a) 216 cells (left of figure) and (b) 64 cells (right of figure).

small changes in resistivity. In the lower part of Fig. 5 we present the numerical results obtained by Dey & Morrison (finite-difference algorithm), Das & Parasnis (moment method, 64 cells) and EL3DQUB (256 cells). A very good agreement can be seen, especially with the results of Dey & Morrison (the maximum difference is less than 1.2 Ωm) and thus validates our program code.

In Fig. 6 we have displayed a grey-scale representation of the pseudo-section computed with EL3DQUB (256 cells) in Fig. 5. Only anomalous resistivities are presented (i.e. computed resistivities minus apparent resistivities in a homogeneous two-layer case).

3-D INVERSE PROBLEM: WHICH APPROXIMATIONS?

The 3-D inversion process is heavy in computing time and power. It necessitates starting from a first estimation of the

(a)

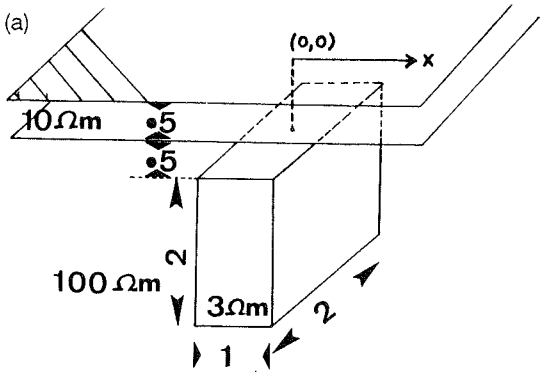

(b)

Number of cells	Dim[1]	x=-3	x=-2	x=-1	x=0
1x2x2 = 4	L	46.14	45.90	46.67	46.91
2x4x4 = 32	.5L	45.91	45.89	46.61	46.85
4x8x8 = 256	.25L	45.76	45.69	46.39	46.63
5x10x10 = 500	.20L	45.80	45.84	46.55	46.79
DAS = 64		44.4	42.0	41.7	42.2

Apparent resistivities for quadripole 6L
1 : size of the cells

(c)

X = -6 . -5 . -4 . -3 . -2 . -1 . 0

								Resistivity of homogeneous layered earth
L	EL3	16.61	16.63	16.68	16.79	16.73	16.05	16.60 Ωm
	Das	16.6	16.6	16.7	16.7	16.7	16.2	
	Dey	16.7	16.5	16.5	16.5	16.6	16.1	
2L	EL3	25.35	25.46	25.70	25.44	23.78	23.04	25.27 Ωm
	Das	25.3	25.4	25.6	25.4	24.2	23.7	
	Dey	25.6	25.9	25.4	25.9	24.1	22.7	
3L	EL3	32.90	33.25	32.73	30.38	29.51		32.58 Ωm
	Das	32.8	33.1	32.7	30.9	30.5		
	Dey	33.7	33.9	33.5	31.9	29.3		
4L	EL3	39.75	38.96	36.16	35.50	35.64		38.88 Ωm
	Das	39.6	39.0	36.8	36.4	36.8		
	Dey	41.0	40.6	37.4	35.9	35.9		
5L	EL3	44.36	41.25	40.88	41.32			44.37 Ωm
	Das	44.4	42.0	41.7	42.2			
	Dey	47.0	42.8	40.6	40.9			
6L	EL3	45.76	45.69	46.39	46.63			49.20 Ωm
	Das	46.6	46.5	47.1	47.4			
	Dey	46.3	45.9	45.3	46.0			
7L	EL3	49.99	50.88	51.29				53.47 Ωm
	Das	50.8	51.5	51.8				
	Dey	50.9	51.4	51.8				

Figure 5. Model used for the computations in (b) and (c). (b) Convergence of the solution given by EL3DQUB when increasing the numbers of cells from 4 to 500. (c) Comparison between the results obtained by the moment method through (EL3) our program (EL3DQUB) with 256 cells, (DAS) a similar program by Das & Parasnis (1987) with 64 cells, and (DEY), a finite-difference algorithm (Dey & Morisson 1979).

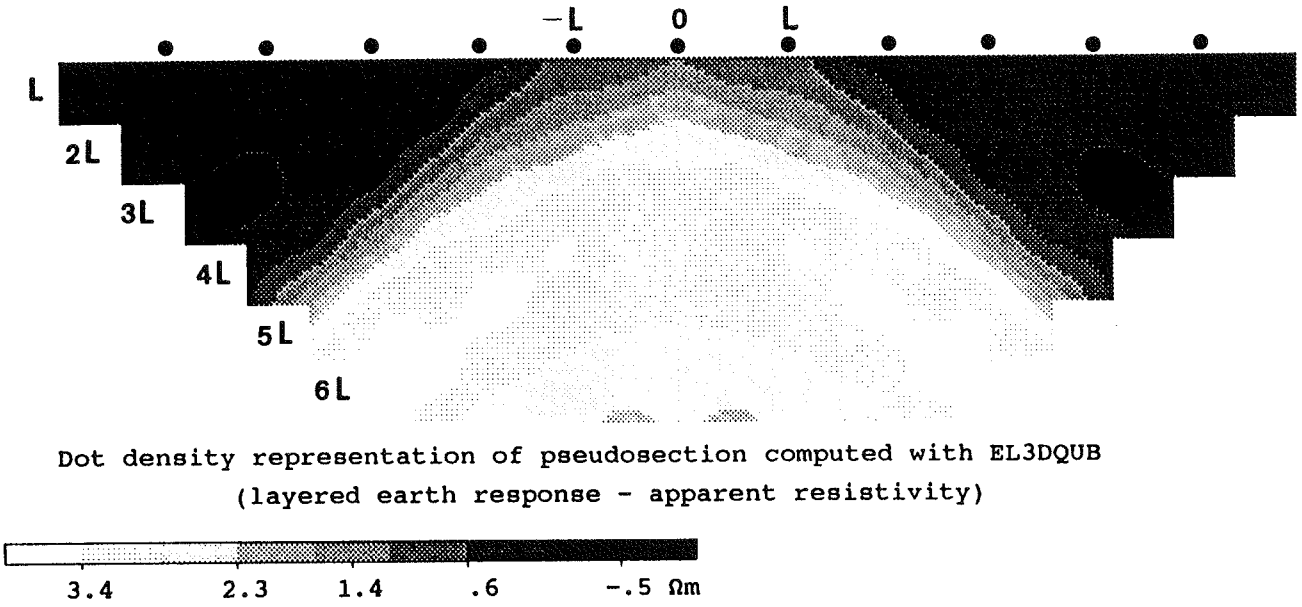

Figure 6. Grey-scale representation of the pseudo-section computed with EL3DQUB (numerical results and model in Fig. 5).

parameter values to calculate by direct modelling the theoretical results and also the sensitivity matrix (Jacobian). Then, by applying an inversion procedure, one calculates the variations of these parameters that minimize a distance between the observations and the model results. This series of operations is then repeated until a criterion for convergence is fulfilled.

To simplify the calculation, it is possible to reduce the number of parameters or to redefine the convergence criterion, and this possibility will be considered later. We also have to consider approximations based upon physical processes that may simplify the direct modelling and/or the calculation of the jacobian.

The first approximation to be considered is usually called the 'Born approximation': it assumes that $\mathbf{E} \simeq \mathbf{E}_p$ in each cell. There is no matrix inversion in the direct problem, which then reduces to a simple 3-D integration. Because the results become linearly dependent upon the conductivity of each cell, there is no need of iteration or jacobian determination when the geometry of the cells remains fixed. This approximation corresponds to the omission of the demagnetizing field in magnetism. Some authors have made this assumption (Noel & Xu 1991). It seems reasonable to use it only when small contrasts of resistivity are encountered however. Unfortunately, the resistivity contrast is often high, even in shallow-depth prospecting. To test the impact of this Born approximation, we have considered a simple model (Fig. 7), where a conductive body made of an upper part of resistivity 30 Ωm and a lower part of resistivity 15 Ωm is imbedded in a homogeneous medium of resistivity 100 Ωm. Each part is 0.5 length-units thick and the top of the body is 0.5 from the ground surface. The horizontal section of the heterogeneity is 3×3 and is divided into 72 cells. The variations of the apparent resistivity for a classical Wenner array with a 2-interprobe spacing is depicted in Fig. 7. A huge difference can be observed between the calculation without approximation (triangles) and the Born approximation (stars). The maximum of the anomaly differs from 61 to 22 Ωm. The difference is confirmed by the values of the electric field inside the body (Table 1): the total field is about one-half of the primary one.

Another approximation was proposed recently (Habaschy & Spies 1993) for electromagnetic scattering. It is based upon the observation that, in the matrix expression, the diagonal terms are greater than the others. Non-diagonal terms are zeroed in this approximation: physically, the influence of a cell upon itself is greater than cross-coupling between cells. This approximation is is called the 'localized non-linear approximation' (LN); localized because the cross-coupling is neglected, and non-linear because the dependence of the anomaly on the conductivity contrast is non-linear. The response of the model under this approximation is presented in Fig. 7; the variation from the exact shape of the anomaly remains within a 10 per cent limit in amplitude, but the lateral variations are smoothed. In Table 1, we have also shown the value of the electric field within the central cells of the body. The change from total field is very small for the upper 30 Ωm layer, but it is about 50 per cent in the centre of the more conductive, lower layer.

In the case of two resistive bodies (300 Ωm for the upper bodies and 600 Ωm for the lower bodies), the response computed with the Born approximation is much more similar to the response calculated with the LN approximation (Fig. 8) than the response of a conductive body. Nevertheless, their amplitudes are quite different from the real case (see Table 2), and we conclude that these approximations cannot be used in our case.

INVERSION SCHEME

The general discrete inverse problem consists of inferring the model parameters from the apparent resistivities measured with different quadripoles. We have chosen a model with a limited number of parameters, namely N

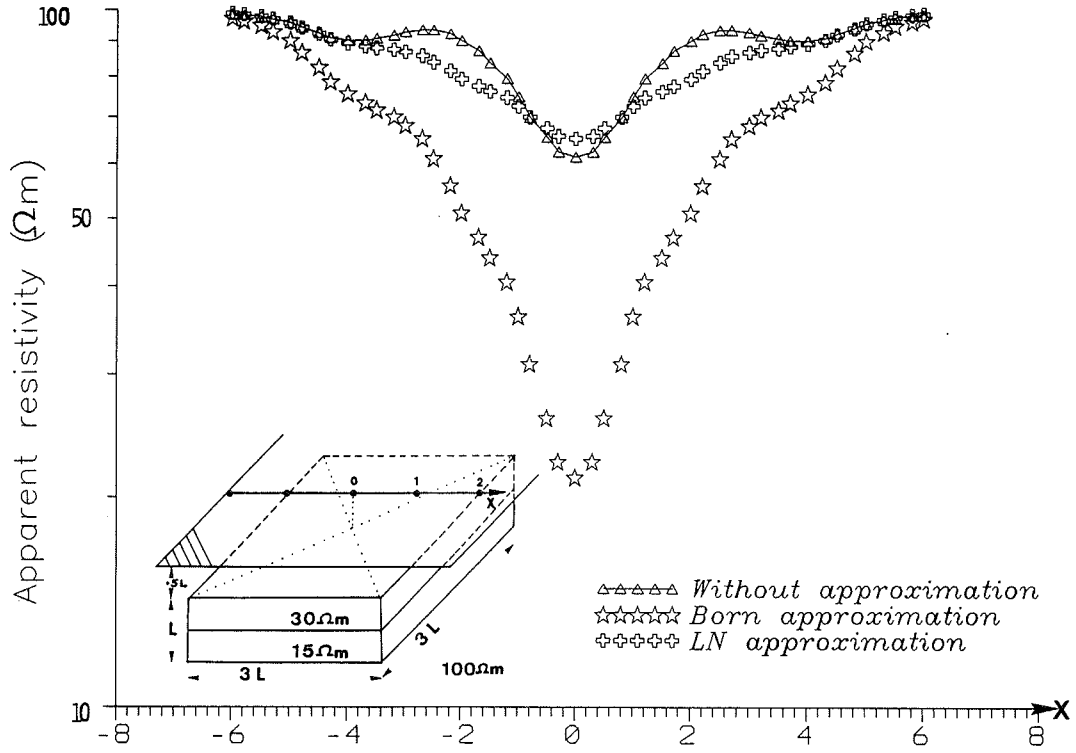

Figure 7. Comparison of the electrical response of a conductive body on a profile: with the Born approximation, with the LN approximation and without an approximation.

Table 1. Comparison between the primary electrical field ($\mathbf{E}_p$) and secondary electrical field using the Born approximation ($\mathbf{E}_t$) and LN approximation ($\mathbf{E}_{LN}$). Case of a conductive body.

Case of a conductive body

Electric field (V/m) in the cells of the upper part (30 Ωm)

X	-6	-4	-2	+2	+4	+6
E_t	-2.43	-2.00	-1.79	-1.79	-2.00	-2.43
E_p	-4.77	-3.70	-3.25	-3.25	-3.70	-4.77
E_{LN}	-2.67	-2.07	-1.82	-1.82	-2.07	-2.67

Electric field (V/m) in the cells of the lower part (15 Ωm)

X	-6	-4	-2	+2	+4	+6
E_t	-1.33	-1.59	-1.66	-1.66	-1.59	-1.33
E_p	-3.52	-3.03	-2.79	-2.79	-3.03	-3.52
E_{LN}	-1.21	-1.05	0.96	0.96	-1.05	-1.21

resistivities: the half-space is discretized as in the forward problem into N small cubic cells with a fixed geometry (constant size). Taking a size as small as we wish, there is no lack of generality and the model space can be represented by a finite set of N (true) resistivities. Taking the same discretization of space between the direct and inverse problem is a simplification of our code. We should in the future increase, for example, the numbers of layers beyond the heterogeneous region and in the homogeneous background. Moreover, this should remove the implicit assumption made in our inverse modelling whereby the real changes of resistivities (direct problem) coincide with the space discretization of the inverse problem.

Several mathematical methods and algorithms used to solve this problem are reviewed hereafter, but only a few of them are applicable to the electrical inverse problem.

(1) Back-projection: this technique is often used in the exploration of the human body by X- and gamma-ray analysis, or in the seismology. It consists of distributing equally the perturbation (equal to the difference between the observed data and a modelled set of data) along ray paths which can be linear or curved. This procedure is repeated for all ray paths. It has the advantage of being very fast but it is based on assumptions that we cannot support in our case: (i) theoretical parametrization by rays in electrical methods makes no sense when diffusion equations apply; (ii) the geometry of the rays is often fixed and does not change when the resistivities of the cells are changed; (iii) this method works properly when at least three or four free surfaces around the anomalous region can be used for making measurements; (iv) back-projecting the perturbation equally along the ray path results in a well known 'blurring effect' when significant resistivity contrasts are encountered, which is almost always the case in subsurface surveying: no sharp resistivity reconstruction can be obtained as pictured, for example, in the article by Noel & Xu (1991). We think that this method should be used only as an a priori resistivity model for other inversion methods (Shima 1992).

(2) Filtered back-projection (or convolution method): this is similar to back-projection, except that each ray is filtered before being back-projected. This technique should counterbalance the blurring effect, but this does not remove the assumptions (i) to (iii) previously mentioned.

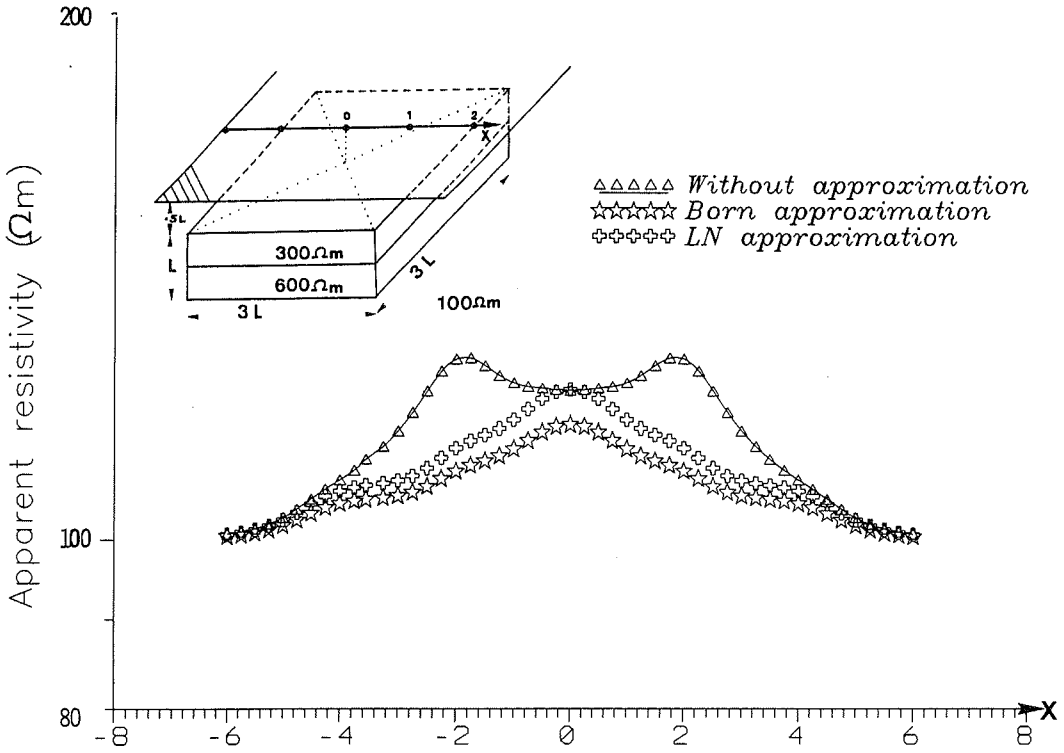

Figure 8. Comparison of the electrical response of a resistive body on a profile: with the Born approximation, with the LN approximation and without an approximation.

Table 2. Comparison between the primary electrical field ($\mathbf{E}_p$) and secondary electrical field using the born approximation ($\mathbf{E}_t$) and LN approximation ($\mathbf{E}_{LN}$). Case of a resistive body.

Case of a resistive body

Electric field (V/m) in the cells of the upper part (300 Ωm)

X	-6	-4	-2	+2	+4	+6
E_t	-6.65	-4.52	-4.06	-4.06	-4.52	-6.65
E_p	-4.77	-3.70	-3.25	-3.25	-3.70	-4.77
E_{LN}	-6.15	-4.77	-4.19	-4.19	-4.77	-6.15

Electric field (V/m) in the cells of the lower part (600 Ωm)

X	-6	-4	-2	+2	+4	+6
E_t	-5.72	-3.37	-3.10	-3.10	-3.37	-5.72
E_p	-3.52	-3.03	-2.79	-2.79	-3.03	-3.52
E_{LN}	-4.88	-4.21	-3.87	-3.87	-4.21	-4.88

(3) Algebraic reconstruction techniques (ART): in these methods, the corrections are applied to each cell along a ray and repeated, the same correction being made to the remaining rays. In SIRT (simultaneous reconstruction technique), the correction for one cell is the summation of elementary corrections corresponding to all the rays that pass through that cell. These methods can give reliable results in a short period of computer time but suffer from the low number of rays available in subsurface electrical imaging (only ground/air interface is used in general).

(4) The most widely used method is some kind of iterative least-squares technique, which is strictly valid only for Gaussian errors (errors in the observed resistivities, in the modelling of the direct problem, and in the given a priori model); see Al-Chalabi (1992).

Let $\mathbf{m}$ be the model parameters (set of true resistivities), $\mathbf{d}$ the data (observable apparent resistivities) and G an operator from M into D (lowercase letters for a set of values (chart) and uppercase letters for the corresponding space), then

$$\mathbf{d} = G\mathbf{m}$$

(Tarantola 1987). As the problem is not linear, we have to linearize it by a Taylor series approximation around an estimated set of the model parameters $\mathbf{m}_e$:

$$G\mathbf{m} = G\mathbf{m}_e + \sum_{i=1}^{n} \mathscr{A}_i(\mathbf{m} - \mathbf{m}_e)^i \quad \text{with} \quad \mathscr{A}_i = \left[\frac{\partial^i G}{\partial \mathbf{m}^i}\right]_{\mathbf{m}_e}. \tag{10}$$

When considering only the first partial derivative term, we have

$$G\mathbf{m} \simeq G\mathbf{m}_e + \left[\frac{\partial G}{\partial \mathbf{m}}\right]_{\mathbf{m}_e}(\mathbf{m} - \mathbf{m}_e), \tag{11}$$

$$G\mathbf{m} - G\mathbf{m}_e = \mathbf{d} - G\mathbf{m}_e \simeq \mathscr{G}(\mathbf{m} - \mathbf{m}_e). \tag{12}$$

$\mathscr{G}$, made of the first-order partial derivatives, is called the sensitivity matrix (or the Jacobian of the operator G): it relates the change between the model parameters $(\mathbf{m} - \mathbf{m}_e)$ and the change between the observed data $(\mathbf{d})$ and calculated data $G\mathbf{m}_e$. Let $\Delta\boldsymbol{\rho}$ be $(G\mathbf{m} - G\mathbf{m}_e)$ and $\Delta\mathbf{m}$ the change in the model parameters we are looking for: $\Delta\boldsymbol{\rho} = \mathscr{G}\Delta\mathbf{m}$.

This system of equations can be over- or underdetermined depending on the ratio between the number of measurements and the number of unknowns. We shall consider only overdetermined problems, since we manage in the fields to obtain more measured, apparent resistivities than unknown, true resistivities of cells. Moreover, in our case we cannot evaluate at present both modelling and measurements errors, and consequently the general inverse solution as defined by Tarantola (1987) cannot be applied as such.

No direct inversion of matrix $\mathcal{G}$ can be performed because the inversion of $\mathcal{G}$ is usually unstable (nearly null eigenvalues). These eigenvalues arise from an ill-posed problem, due to insufficient data for some cells and/or problems of electrical equivalence. Some regularization technique must be used (Tikhonov & Arsenin 1977) either by truncation (zeroing elements of the matrix) or by reducing ('damping') the effect of undetermined parameters (basis of methods like ridge regression or damped least-squares) prior to the inversion. Some a priori information about the solution can also be added through the formalism of Lagrange multipliers, for example.

The method we have applied has been developed by Levenberg (1944) and Marquardt (1963). The main idea is to limit the changes in the model parameters by using a cost function:

$$S = \Delta\boldsymbol{\rho}^{\mathrm{T}}\Delta\boldsymbol{\rho} + \lambda\Delta\mathbf{m}^{\mathrm{T}}\Delta\mathbf{m}.$$

Differentiation with respect to the model parameter $\Delta\mathbf{m}$ and equating to zero gives

$$(\mathcal{G}^{\mathrm{T}}\mathcal{G} + \lambda\mathbf{I})\Delta\mathbf{m} = \mathcal{G}^{\mathrm{T}}\Delta\boldsymbol{\rho},$$

and thus

$$\Delta\mathbf{m} = (\mathcal{G}^{\mathrm{T}}\mathcal{G} + \lambda\mathbf{I})^{-1}\mathcal{G}^{\mathrm{T}}\Delta\boldsymbol{\rho}. \quad (15)$$

The multiplier λ was termed a 'damping' factor by Levenberg in (1944) and consequently this method belongs to the class of the diagonal damped least-squares problems.

When λ is large, the matrix $(\mathcal{G}^{\mathrm{T}}\mathcal{G} + \lambda\mathbf{I})$ becomes diagonally dominant and this method is similar to the steepest descent method, while λ small implies the ordinary least-squares (LS) method.

Generally, λ is set to an arbitrary high value for the first iteration and then reduced by multiplication by a constant factor (<1), and the new cost function is computed. If the new cost function has been lowered, then parameters are updated and λ is lowered; otherwise, there is no change in the model parameters and λ is multiplied by the inverse of the constant.

In order to stabilize and accelerate the convergence of the inversion process, two regularizations have been used: (i) calculated resistivities must always be positive and (ii) the calculated spatial distribution of resistivities must be 'smooth'. We will explain later the implementation of these two constraints.

APPLICATION TO THEORETICAL CASES

As already mentioned, the ground is represented by two layers of cells imbedded in a homogeneous medium. The cells are of cubic shape and their resistivities constitute the parameters of the model. The lateral extent of the heterogeneities is defined by $3L$, which constitutes the width and the length of the meshed volume.

To limit the computing time, we choose 25 cells ($0.6L$ in length) in the first layer and 9 cells (L in length) in the second (Fig. 9). The resistivity of the surrounding medium is 100 Ωm and the thickness of the overburden is $0.3L$. For the data, we have calculated the apparent values of the resistivities on a regular grid (7×7) for a quadripole in Wenner configuration for interelectrode distances, a, of L, $2L$ and $3L$. We then obtain 147 data for determining the resistivities of 34 cells. The aim of this paper is not to answer the question of how many data are sufficient for making the inversion process stable, this will be discussed in a forthcoming article.

We have treated, in order, the case of a vertical contrast between the two layers of cells, the case of a horizontal contrast and the more complex case with both vertical and horizontal variations. Finally, the event of noisy data has been treated.

Numerically, we followed the scheme of the Levenberg–Marquardt algorithm (Press *et al.* 1992) with a Lagrangian

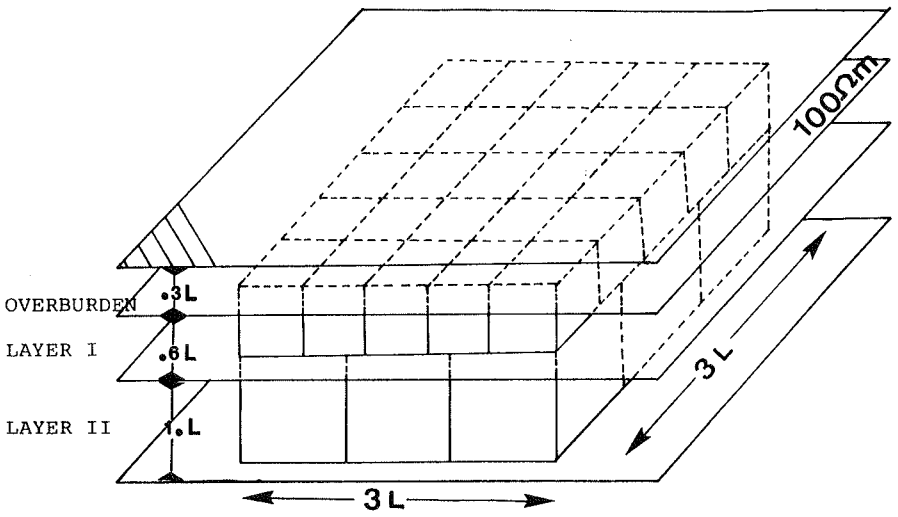

Figure 9. Model used for the inversion scheme.

multiplier λ starting at an arbitrary value of 0.001. At each step of the iterative process, we calculate S (sum of the squared differences between observed and calculated apparent resistivities). If the value of S increases, λ is increased by a factor of 10. If, on the other hand, S decreases, λ is divided by the same factor. The iterations are stopped when S/N is lower than 2 (arbitrarily). The number of successive changes of λ is limited to seven and the maximum number of iterations is normally limited to 32. When λ has a low value, it plays a negligible part and the scheme is a least-squares one (LS). When λ is high, the scheme is of steepest descent type.

We also limit the resistivity to positive values by forcing the resistivity to an arbitrary value of 1 Ωm when the calculated resistivity is negative. To reduce lateral oscillations of the resistivity from one cell to another, we apply at each iteration a spatial 2-D median filtering on a (3×3) mesh by substituting each cell's resistivity by the median value computed with its eight nearest neighbours. This last process is not necessary for convergence but accelerates the convergence towards the solution.

We first tested the LN approximation for the first five iterations. In no case has it accelerated the convergence, and it even leads to divergence when the cells are more resistive than the medium. This can be explained by the significant differences that exist between LN and complete calculations for the lateral variations of the anomalies (see Figs 7 and 8).

Conductive vertical contrast

We first tested the case where the first layer has a 100 Ωm resistivity equal to that of the surrounding medium. For the second layer, the resistivity is 40 Ωm. In Fig. 10 we represent the variations of S and those of the resistivities of the two layers (ρ_{sup} and ρ_{inf}) versus the number of iterations. 'Error bars' represent, in fact, the span between the maximum and minimum values of the calculated resistivities. The a priori resistivities are 90 and 80 Ωm. We observe that the convergence necessitates 11 iterations, but, as the resistivity of the first layer oscillates, that of the lower layer reaches an accuracy of 10 per cent in seven iterations. At the seventh iteration, $S = 29$ $(\Omega m)^2$, corresponding to an RMS error of only 0.44 Ωm on the apparent resistivities.

Resistive vertical contrast

As in the preceding case, ρ_{sup} equals 100 Ωm, but the second layer is more resistive, at 400 Ωm. Starting with a priori

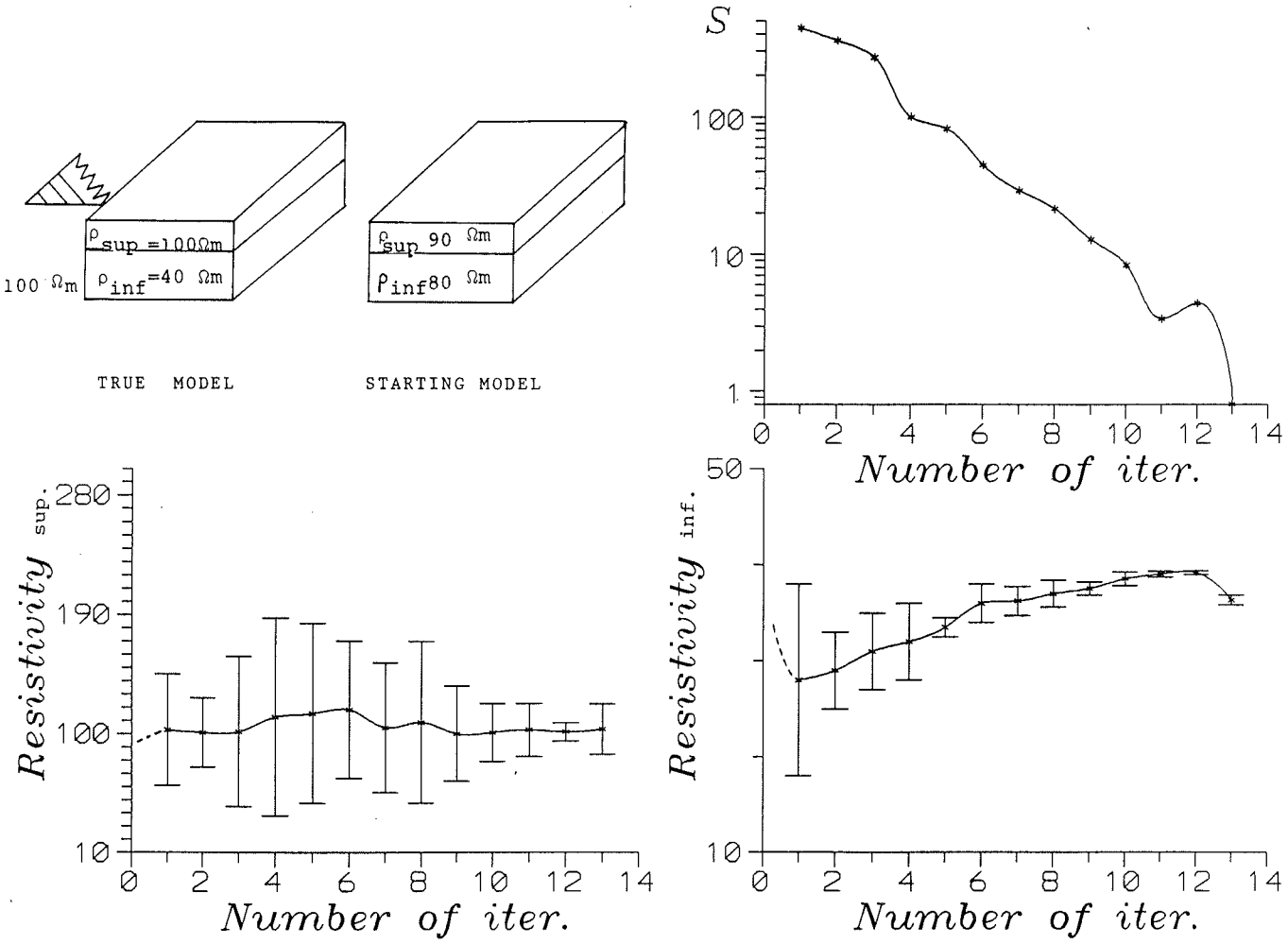

Figure 10. Inversion in the case of a single conductive body embedded in a uniform medium: variations of S and the resistivities of the two layers versus the number of iterations.

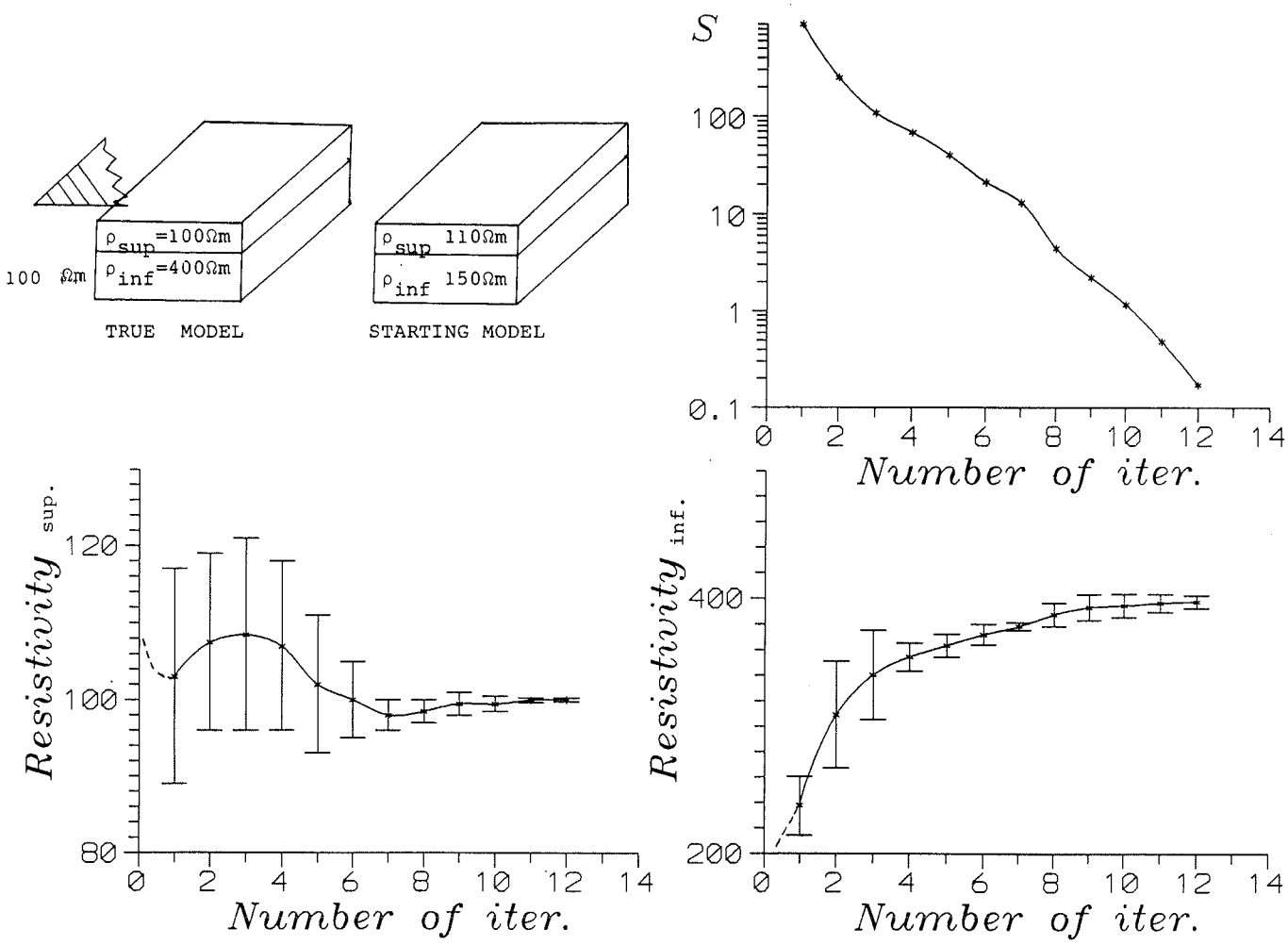

Figure 11. Inversion in the case of a single resistive body embedded in a uniform medium: variation of S and the resistivities of the two layers versus the number of iterations.

resistivities of 110 and 150 Ωm, we obtain (Fig. 11) a 10 per cent difference for ρ_{inf} (360 Ωm) at the fifth iteration, where $S = 40\ (\Omega m)^2$, which corresponds to an RMS error of 0.52 Ωm.

When comparing this with the results Fig. 10, it can be seen that convergence is more rapid for the resistive contrast than for the conducting one.

Two different conductive vertical contrasts

In this case, the first layer has a 10 Ωm resistivity and the second layer a 40 Ωm resistivity. We start with a uniform distribution of 30 Ωm for all the cells. This value corresponds to the minimum value of the apparent resistivities. At the first iteration, the value of S is high: 13 976 $(\Omega m)^2$. It diminishes slowly to reach 1000 at the 14th iteration and 100 at the 42nd iteration (Table 3). We have stopped at the 50th iteration, where the RMS error is 0.57 Ωm for the apparent resistivities. Computed values for ρ_{sup} range between 9.4 and 9.6 Ωm and between 39.8 and 39.9 Ωm for ρ_{inf}. The 10 per cent limit was reached at the 18th iteration for ρ_{sup} and at the 43rd for ρ_{inf}.

Two different mixed vertical constrasts

In this model, ρ_{sup} equals 200 Ωm and ρ_{inf} equals 50 Ωm. Starting values are 120 and 95 Ωm (*extrema* of the apparent resistivities for $a = L$ and $a = 3L$). We observe a quicker

Table 3. Variations of S when considering a resistive body (40 Ωm) under a conductive body (10 Ωm).

Iter	1	2	3	4	5	6	7	8	9	10	11	12	13
S	8166	7015	5190	4549	3762	3280	2709	2288	2017	1792	1574	1358	1140

Iter	14	15	16	17	18	19	20	–	25	30	35	40	45	50
S	960	824	709	618	544	483	434	–	290	218	163	103	60	48

Table 4. Variations of S when considering a conductive body (50 Ωm) under a resistive body (200 Ωm).

Iter	1	2	3	4	5	6	7	8	9	10	11	12	13	14	15	16	17
S	660	162	51	27	22	9.9	8.3	6.5	4.4	1.5	.60	.55	.50	.35	.23	.26	.11

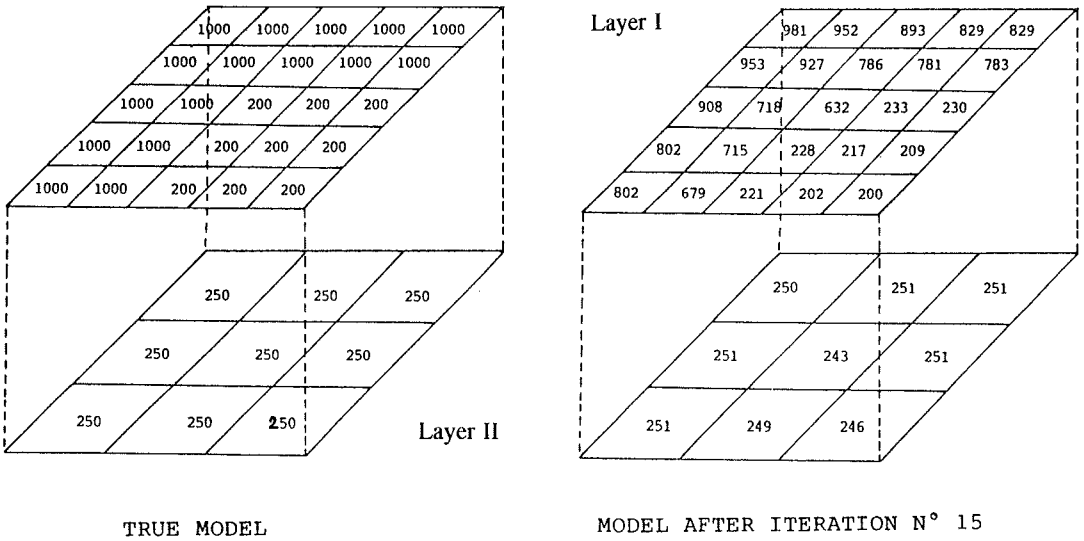

Figure 12. Inversion in the case of a complex model with both vertical and horizontal contrasts: resistive case (left); inverted resistivities for the two layers (right).

convergence (Table 4). At the 17th iteration, S is quasi-nil [0.11 $(\Omega m)^2$] and ρ_{sup} ranges between 198 and 204 Ωm, while ρ_{inf} is uniform and is equal to 49.9 Ωm.

From these first four cases, one can conclude that, in the situation where a resistive feature overlays a conductive one, resistivities are resolved very accurately and with a better precision than in the case where the conductive feature lays over the resistive one. In the latter case, the convergence is also slower, but the determination of the resistivity of the conductive feature is more rapid than that of the underlying resistive one. It exists a screening effect due to conductive features that tend to gather the current lines and mask deeper features.

Both vertical and lateral contrasts: feature more resistive than its surroundings

The geometry of the model is presented in Fig. 12. In layer I, an L-shaped area has a resistivity of 1000 Ωm and the

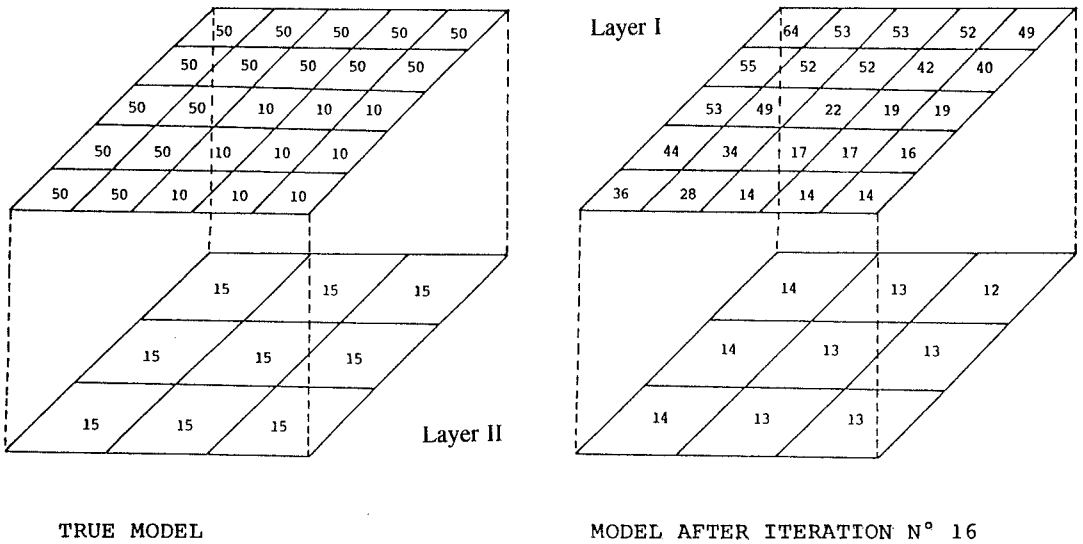

Figure 13. Inversion in the case of a complex model with both vertical and horizontal contrasts: conductive case (left); inverted resistivities for the two layers (right).

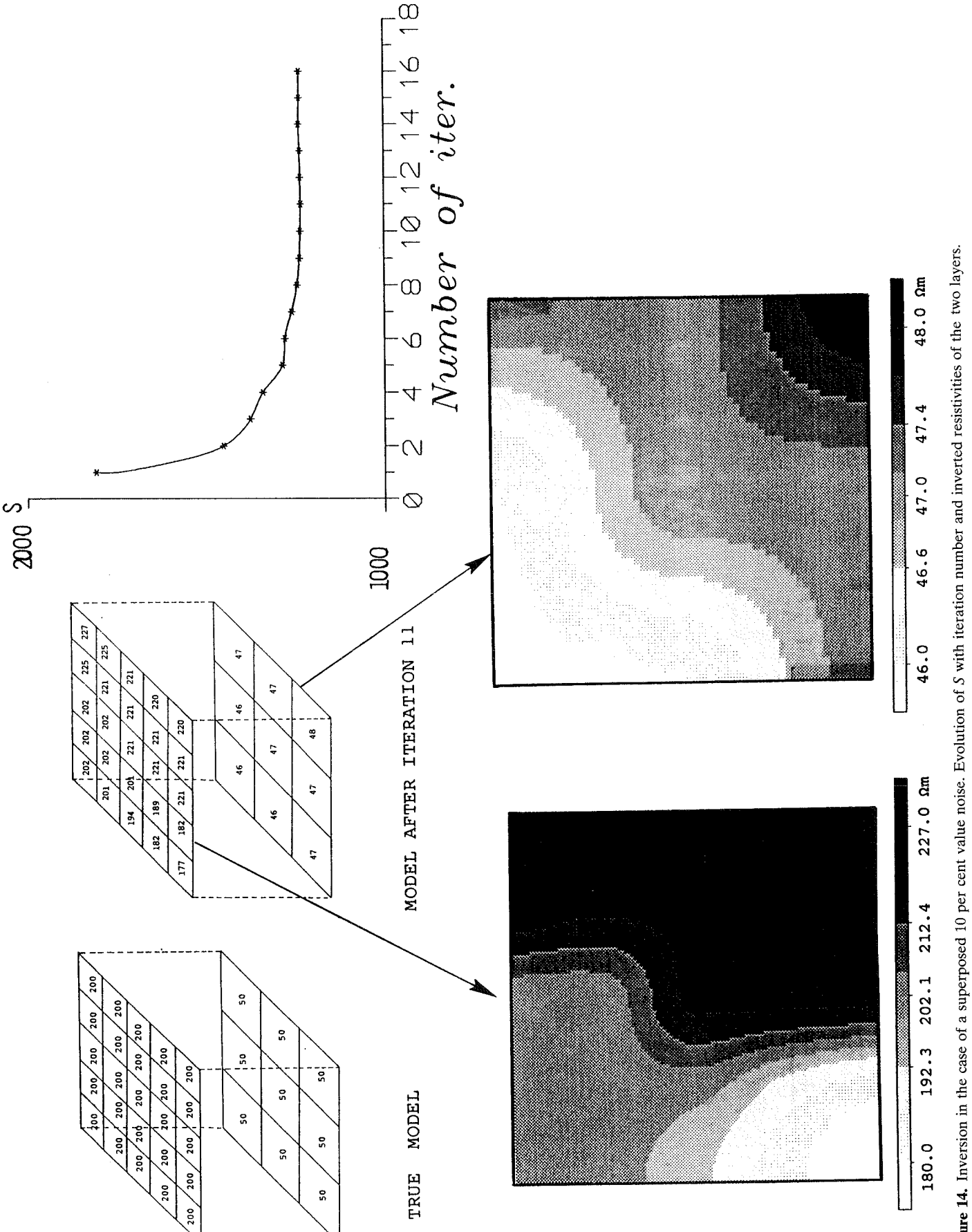

Figure 14. Inversion in the case of a superposed 10 per cent value noise. Evolution of S with iteration number and inverted resistivities of the two layers.

remaining wedge area is at 200 Ωm. Layer II has a uniform resistivity of 250 Ωm. Starting with a uniform value of 800 Ωm for both layers, the value of S decreases to 86 $(\Omega m)^2$ at the 15th iteration. In layer I (Fig. 12), one observes a good agreement with the data values within a 20 per cent limit, except at the corner of the L-shaped area. The agreement is perfect for the second layer: minimum value 243, maximum value 251 Ωm.

Both vertical and lateral contrasts: feature more conductive than its surroundings

In layer I (Fig. 13), we consider an L-shaped area of 50 Ωm and a wedge area of 10 Ωm. In layer II, resistivity is uniform (15 Ωm). Starting from 50 Ωm for all the cells, a minimum value $S = 260\ (\Omega m)^2$ is reached at iteration 16, which corresponds to an RMS error of 1.3 Ωm on the apparent resistivities. As shown in Fig. 13, the wedge resistivity is not well resolved: between 14 and 22 Ωm instead of 10 Ωm. Layer II is found to be more conductive than the correct value (12 to 14 Ωm instead of 15 Ωm).

Again, the conductive case is not resolved as well as the resistive case.

Case with noisy data

We add to the apparent resistivities a random noise of ±5 per cent for the model in which layer I is at 200 Ωm and layer II at 50 Ωm. As can be seen in Fig. 14, showing the variation of S versus number of iterations, the error value tends to stay around $S = 1175\ (\Omega m)^2$, reached at the 11th iteration, and corresponds to an RMS of 2.83 Ωm. This value corresponds exactly to the standard deviation computed from the statistics of the noise introduced in the apparent resistivities.

It is, then, logical to stop the iteration process here. This could lead to a definition of a criterion for stopping the inversion process when real apparent resistivities are used.

The computed resistivities of the cells in level I lie in a 10 per cent interval, most of them being higher than 200 Ωm, while resistivities of the cells in layer II are lower (46 to 48 Ωm) than 50 Ωm. We are therefore in a situation of electrical equivalence.

CONCLUSIONS

The moment method constitutes a good solution to the 3-D direct problem for modelling the resistivities obtained in shallow-depth electrical surveying. We have demonstrated that it is in good agreement with other calculation techniques and physical model studies. It has also a direct physical meaning through the fact that a resistivity can be assigned to a volume which can be discretized in a number of cells with uniform electrical properties. We have already applied this technique to electromagnetic modelling and it is possible to conceive of a joint 3-D inversion of electromagnetic and electrical data in the near future.

The least-squares inversion scheme we have used is a classical concept but is still convenient for 3-D resistivity inversion. Still, some constraints must be added to the inversion process to make it more stable and less time consuming. We have shown that, with a fairly small amount of data, reconstruction of the true resistivities is feasible. A great deal of work has still to be done on thinking about the best quadripole spacing and geometry to be used for solving specific problems.

We have shown that approximations such as Born or LN, even if they can drastically lower the amount of time for the computations, cannot be used in the inversion process.

The studies of theoretial cases show that the determination of resistivity for resistive features is more precise than for conductive ones. This confirms the specific interest of the DC electrical method for resistive target characterization.

The application to field data coming from acquisition devices with an automatic scanner for electrodes is now under test and will be presented in a forthcoming paper.

REFERENCES

Al-Chalabi, M., 1992. When least-squares least, *Geophys. Prospect.*, **40,** 359–378.

Alfano, L.M., 1959. Introduction to the interpretation of resistivity measurements for complicated structural conditions, *Geophys. Prospect.*, **7,** 311–368.

Alfano, L.M., 1993. Geoelectrical methods applied to structures of arbitrary shapes, *J. appl. Geophys.*, **29,** 193–209.

Barker, R., 1992. A simple algorithm for electrical imaging of the subsurface, *First Break,* **10,** 53–62.

Barnett, C.T., 1972. Theoretical modelling of induced polarization due to arbitrarily shaped bodies, *PhD thesis,* Colorado School of Mines.

Das, U.C. & Parasnis, D.S., 1987. Resistivity and induced polarization responses of arbitrarily shaped 3-D bodies in a two-layered earth, *Geophys. Prospect.,* **35,** 98–109.

Dey, A., Morrison, H.F., 1979. Resistivity modelling for arbitrarily shaped two-dimension structures, *Geophys. Prospect.,* **27,** 106–136.

Dieter, K., Paterson, N.R. & Grant, F.S., 1969. IP and resistivity type curves for three dimensional bodies, *Geophysics,* **34,** 615–632.

Edwards, L.S., 1977. A modified pseudosection for resistivity and induced-polarization, *Geophysics,* **42,** 1020–1036.

Endo, G., Takeuchi, M. & Matsuzaka, S., 1973. Study on the three-dimensional modeling of strata in electrical prospecting, its experimental equipment and the accuracy of measurements, *Butsuri-Tanko (Geophysical Exploration),* **26,** 1–9 (in Japanese).

Griffiths, D.H. & Turnbull, J., 1985. A multi-electrode array for resistivity surveying, *First Break,* **3,** 16–20.

Griffiths, D.H. & Barker, R.D., 1993. Two-dimensional resistivity imaging and modelling in areas of complex geology, *J. appl. Geophys.* **29,** 211–226.

Habaschy, T.M., Groom, R.W. & Spies, B.R., 1993. Beyond the Born and Rytov approximation: a non linear approach to electromagnetic scattering, *J. geophys. Res.,* **98,** 1759–1775.

Hesse, A., Jolivet, A. & Tabbagh, A., 1986. New prospects in shallow depth electrical surveying for archaeological and pedological applications, *Geophysics,* **51,** 585–594.

Hohmann, G.W., 1975. Three-dimensional induced polarization and electromagnetic modelling, *Geophysics,* **40,** 309–324.

Keller, G.V. & Frischknecht, 1966. *Electrical methods in Geophysical Prospecting,* Pergamon Press, Oxford.

Lee, T., 1975. An integral equation and its solution for some two- and three-dimensional problems in resistivity and induced polarization, *Geophys. J. R. astr. Soc.,* **42,** 81–95.

Levenberg, K., 1944. A method for the solution of certain nonlinear problems in least squares, *Q. appl. Math.,* **2,** 164–168.

Li, Y. & Oldenburg, D.W., 1992. Approximate inverse mapping in DC resistivity problems, *Geophys. J. Int.,* **109,** 343–362.

Marquardt, D.W., 1963. An algorithm for least square estimation of non-linear parameters, *J. Soc. Indust. appl. Math.* **11,** 431–441.

Mufti, I.R., 1978. A practical approach to finite-difference resistivity modeling, *Geophysics,* **43,** 930–942.

Noel, M. & Xu, B., 1991. Archaeological investigation by electrical resistivity tomography: a preliminary study, *Geophys. J. Int.,* **107,** 95–1102.

Okabe, M., 1981. Boundary element method for the arbitrary inhomogeneities problem in electric prospecting, *Geophys. Prospect.,* **29,** 39–59.

Okabe, M., 1982. Reciprocical averaging techniques in the geoelectrical boundary element approach, *Geophys. Prospect.,* **30,** 653–672.

Park, S.K. & Van, G.P., 1991. Inversion of pole pole data for 3-D resistivity structure beneath arrays of electrodes, *Geophysics,* **56,** 951–960.

Pelton, W.H., Rijo, L. & Swift, C.M., Jr, 1978. Inversion of two-dimensional resistivity and induced-polarization data, *Geophysics,* **43,** 788–803.

Petrick, W.R., Jr, Sill, W.R. & Ward,, S.H., 1981. Three-dimensional resistivity inversion using alpha centers, *Geophysics,* **46,** 1148–1163.

Poirmeur, C. & Vasseur, G., 1988. Three-dimensional modeling of a hole-to-hole electrical method: application to the interpretation of a field survey, *Geophysics,* **53,** 402–414.

Press, W.M., Flannery, B.P., Teukolsky, S.A. & Vetterling, W.T., 1992. *Numerical Recipes,* Cambridge University Press, Cambridge.

Pridmore, D.F., Hohmann, G.W., Ward, S.H. & Sill, W.R., 1981. An investigation of finite-element modeling for electrical and electromagnetic data in three dimensions, *Geophysics,* **46,** 1009–1024.

Raiche, A.P., 1974. An integral equation approach to three-dimensional modelling, *Geophys. J. R. astr. Soc.,* **36,** 363–376.

Sasaki, Y., 1989. Two-dimensional joint inversion of magnetotelluric and dipole–dipole resistivity data, *Geophysics,* **54,** 254–262.

Scriba, H., 1981. Computation of the electric potential in three-dimensional structures, *Geophys. Prospect.,* **29,** 790–802.

Shima, H., 1990. Two-dimensional automatic resistivity inversion technique using alpha centers, *Geophysics,* **55,** 682–694.

Shima, H., 1992. 2-D and 3-D resistivity image reconstructing using crosshole data, *Geophysics,* **57,** 1270–1281.

Smith, N.C. & Vozoff, K., 1984. Two-dimensional DC resistivity inversion of dipole–dipole data, *IEEE Trans. Geoscience Rem. Sens.,* GE-22, pp. 21–28.

Spahos, J., 1979. Calculs sur modèle et rôle du quadripôle en prospection électrique de subsurface. Application à la détection archéologique, *Thèse de 3ème cycle,* Université P. & M. Curie, Paris.

Tabbagh, A., 1985. The response of a three-dimensional magnetic and conductive body in shallow depth electromagnetic prospecting, *Geophys. J. R. astr. Soc.,* **81,** 215–230.

Tarantola, A., 1987. *Inverse problem theory,* Elsevier, Amsterdam.

Tikhonov, A. & Arsenin, V., 1977. *Solution of ill-posed problems,* John Wiley and Sons, Washington DC.

Tripp, A.C., Hohmann, G.W. & Swift, C.M., 1984. Two-dimensional resistivity inversion, *Geophysics,* **49,** 1708–1717.

Weidelt, P., 1975. Inversion of two-dimensional conductivity structures, *Phys. Earth. planet. Inter.,* **10,** 282–291.